ACS OMEGA

Open Access

http://pubs.acs.org/journal/acsodf

Article

Study on Formation and Migration Law of Foam in Fractures and Its Influencing Factors

Jinghui Li, Yibo Feng, Jianhai Wang, Zhengxiao Xu,* Binfei Li, and Chao Zhang*

Cite This: *ACS Omega* 2024, 9, 24362−24371

Read Online

ACCESS | Metrics & More | Article Recommendations

ABSTRACT: This study focuses on the characteristics of foam generation, flow, and plugging in different reservoir fracture environments. Through visual physical model experiments and stone core displacement experiments, we analyze the flow regeneration of foam in a simulated reservoir fracture environment as well as its sealing and sweeping mechanisms. The findings reveal that low permeability reservoirs, with their smaller and more intricate fracture structures, are conducive to the generation of high-strength foam. This is due to the stronger shear effect of these fracture structures on the injected surfactant and gas mixture system, resulting in a denser foam system. Consequently, low permeability reservoirs facilitate a series of mechanisms that enhance the fluid sweep efficiency. Furthermore, the experiments demonstrate that higher reservoir fracture roughness intensifies the shear disturbance effect on the injected fluid. This disturbance aids in foam regeneration, increases the flow resistance of the foam, and helps to plug high permeability channels. As a result, the foam optimizes the injection-production profile and improves the fluid sweep efficiency. Stone core displacement experiments further illustrate that during foam flooding, the foam liquid film encapsulates the gas phase, thereby obstructing fluid channeling through the Jamin effect. This forces the subsequently injected fluid into other low-permeability fractures, overcoming the shielding effect of high-permeability fractures on low-permeability fractures. Consequently, this improves the fluid diversion rate of low permeability fractures, effectively inhibiting fluid cross-flow and enhancing sweep efficiency. These experimental results highlight the advantages of foam flooding in the development of complex reservoirs with low permeability fracture structures, demonstrating its efficacy in inhibiting fluid cross-flow and optimizing the injection-production profile.

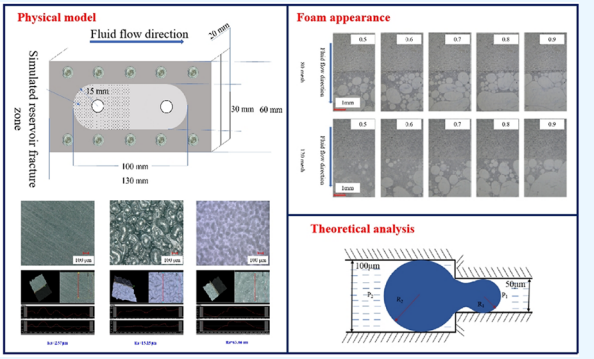

1. INTRODUCTION

In the process of reservoir development, the fluid injected for oil displacement cannot reach the target reservoir effectively due to the heterogeneity of the formation fracture structure. These fluids often bypass formation through large fractures with high permeability in the late stage of oil production, resulting in a cross-flow effect. This condition leads to low fluid utilization efficiency, unsatisfactory sweep efficiency, and a sharp decline in oil production efficiency.[1] Therefore, researchers have explored using a special fluid system to block the high permeability channel during the injection process, inhibit the cross-flow of fluid, and regulate the flow path of subsequent injection. Based on these ideas, a nitrogen foam flooding technology system has been developed. Since foam flooding theory was proposed in the 1960s, this technology system has shown advantages in various reservoir development cases with complex reservoir fracture structures. The foam has multiple mechanisms, such as sealing high-permeability fractures, controlling fluid cross-flow, adjusting the injection-production profile, reducing oil viscosity, and improving the oil displacement mobility ratio.[2−5] The system is particularly effective in improving the fluid sweep efficiency and oil displacement efficiency in the gas flooding process. Based on the particularity of the gas−liquid two-phase structure, the foam effectively encapsulates nitrogen and blocks the high permeability channels based on the superimposed Jamin effect during the flow process to inhibit the loss of nitrogen from these channels. At the same time, due to the resistance effect brought by the above blocking effect, the flow resistance of nitrogen is increased, and it is forced to enter the blind end of complex fractures that were previously difficult to sweep, to improve the sweep efficiency.[6−8] In addition, with foam with the surfactant as the foaming component, based on its existence, the foam system can exert a wettability reversal effect on reservoir fractures and weaken the hydrophobicity of reservoir rocks. Under this condition, the adhesion work

Received: December 30, 2023
Revised: April 17, 2024
Accepted: April 22, 2024
Published: May 30, 2024

required by the fluid to peel the oil from the fracture wall is reduced, and the oil displacement efficiency is optimized.[9,10] Combined with the aforementioned improvement of sweep efficiency, conditions are created for the improvement of oil recovery.

In conventional water flooding and gas flooding, there is a competitive effect between large-sized high permeability fractures and small-sized low permeability fractures in the fracture environment of the reservoir to accommodate the injected oil displacement fluid.[11−14] Due to the high permeability of large fractures, injected fluid tends to flow first from inside them. When the flow path of the fluid in the high permeability fracture is opened, it will form a shielding effect on the flow of the subsequently injected fluid in the low permeability channel, and the low permeability channel is difficult to introduce into the fluid flow.[15] The flow path opened in the high permeability fracture is the cross-flow channel of the fluid, and the other fractures with small openings and large tortuosity in this stage are difficult to sweep by the fluid.[16−18] In the end, the subsequently injected fluid quickly drains out of the reservoir through this channel and cannot effectively spread to other oil-bearing areas promptly. This situation leads to a low fluid sweep efficiency and difficulty in further improving oil recovery. In order to optimize the flow path of injected fluid and mitigate the shielding effect caused by high permeability cracks, specific measures should be implemented. The foam can effectively obstruct the high permeability channel, thereby augmenting the displacement capability of the fluid in low permeability channels. In addition, considering that reservoir high temperature and high pressure have a negative impact on the stable flow of foam as a thermodynamically unstable system, relevant studies further put forward the idea of adding solid phase particles as stabilizers to optimize the structural strength of foam and ensure the effective foam flooding.[19−21] These particles have the effect of reducing the interfacial tension of the foam liquid film and improving the apparent viscosity of the system, thus creating conditions for further improvement of oil recovery by extending the working life of the foam in the reservoir and optimizing the oil displacement mobility ratio.

At present, the research on nitrogen foam mainly focuses on the overall oil displacement efficiency of the system and the evaluation of macroscopic resistance factors. However, there is limited research on the differences in fluid flow patterns in different complex fracture environments of fractured reservoirs. At the same time, the research on the burst, regeneration, and migration of foam in fractured reservoir environments is not systematic enough.[22,23] Therefore, the reservoir fracture physical model experiment and stone core displacement experiment were designed in this study, and the swept mechanism and fracture plugging characteristics of foam under different reservoir fracture scale conditions were discussed,[24−26] which is aimed at providing data reference for the design of field reservoir development process parameters.

2. EXPERIMENTAL SECTION

2.1. Experimental Materials. In this study, the material used for preparing the foam was N_2 gas, purchased from the Qingdao Tianyuan gas factory, with a purity higher than 99.9%. The YF-1 anionic surfactant, used as the foaming agent, was provided by the fund. Due to the relevant confidentiality agreement, the specific molecular formula of the agent could not be disclosed in this paper. Additionally, deionized water was used as the medium to prepare the foaming agent solution, which was mixed with the surfactant. The mass concentration of the surfactant in the solution was set to 0.2 wt %. Furthermore, three kinds of cellophane paper with different surface roughnesses were used to create different fracture environments in reservoir physical model experiments. To discuss the distribution characteristics of foam in different fractures, stone core models were used as the media to simulate different fractures in the reservoir. The sizes of the fractures in the stone cores were 0.09 0.4, 0.8, and 1.2 mm, respectively. The structural forms of the fractures are shown in Figure 1.

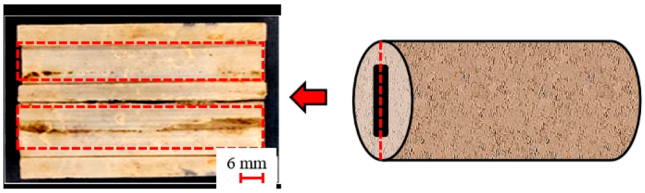

Figure 1. Schematic diagram of stone core model structure.

2.2. Laboratory Apparatus. *2.2.1. Formation Characteristics of Foam Systems in Fractures with Different Roughness.* The ISCO piston pump, manufactured by Teledyne Technologies, had a maximum specified working pressure of 68.95 MPa and a maximum output flow rate of 50 mL·min^{-1}. The acrylic plate reservoir fracture model, purchased from Hua'an Instrument Co., Ltd. (Jiangsu, China), was used in the experiments. The instrument is shown in Figure 2. It was equipped with an inner cavity that is 100 mm long, 30 mm wide, and 4 mm deep. The overall length of the model was 130 mm, the width 60 mm, and the height 20 mm. The gas flowmeter, purchased from Bronkhorst GmbH (Netherlands), could control the maximum gas flow of 20 mL·min^{-1}, with a maximum specified pressure of 2 MPa. Several steel intermediate vessels, drying pipes, check valves, and other ancillary components were used, all produced by Jiangsu Hai'an Petroleum Instrument Co., Ltd., China. In this study, the fluid inside the model was also observed with an ultradepth field microscopic system, which was purchased from Keynes Company (Shanghai Branch, China), and its microscopic magnification range was 0−500 times.

2.2.2. Migration Characteristics of Foam Systems in Fractures with Different Roughness. The instruments used in this part of the work include the ISCO plunger pump, gas flow meter, steel intermediate container, drying pipe, check valve, pressure gauge, and other components, with their specific technical specifications consistent with the instruments used in the previous part of the work. Additionally, this work utilized another acrylic plate reservoir physical model, which was a visual reservoir fracture model composed of two acrylic sheets of the same size and specification. As shown in Figure 3, based on the design ideas of this physical model, laser etching was carried out on the bottom of the inner cavity of the lower cover plate of the acrylic plate model, so that a gap with a length of 100 mm and a width of 15 mm was formed in the middle of the bottom to simulate a straight fracture with a depth of 75 μm. Meanwhile, the upper acrylic plate of the model had a 3 mm threaded opening on the left and right sides of the aperture, serving as the injection end and the outflow end of

https://doi.org/10.1021/acsomega.3c10510
ACS Omega 2024, 9, 24362−24371

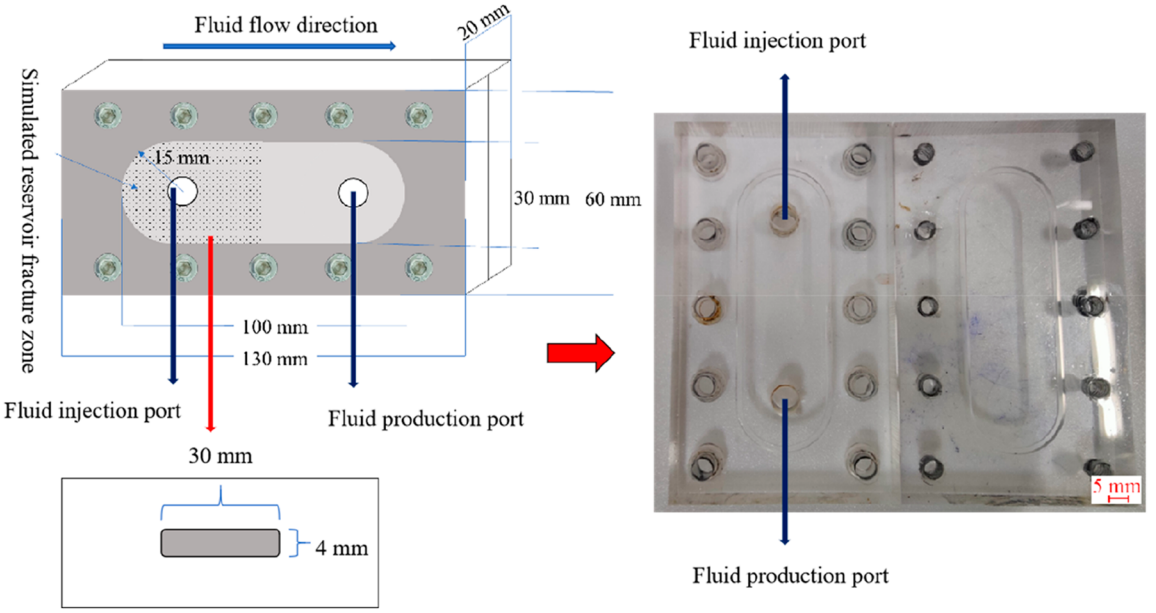

Figure 2. Schematic diagram of the visual microscopic fracture model.

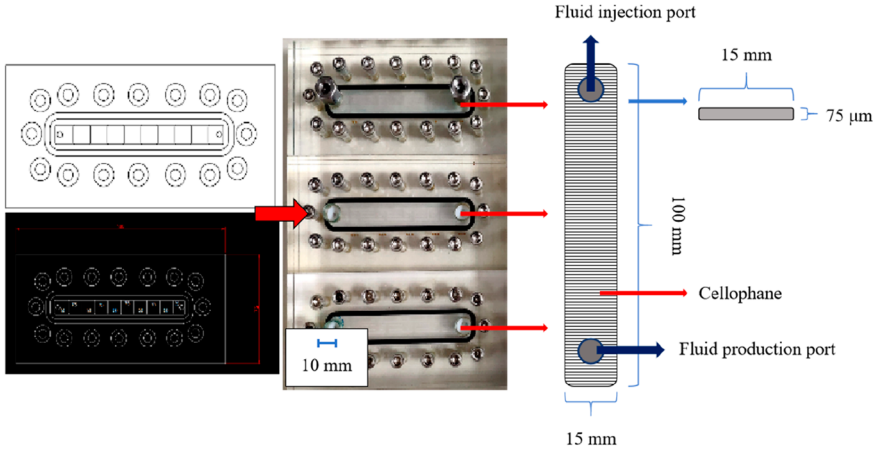

Figure 3. Structure diagram of fracture model with variable opening.

the fluid. The bottom of the acrylic sheet was coated with cellophane of different roughness to simulate the different roughness of the wall. Moreover, in this experiment, the state of the fluid inside the model during the experiment was characterized and scanned in 3D depth by an ultradepth field 3D microscope, as shown in Figure 4. Other experimental equipment used in this part of the study also included accessories, such as foam generators and pressure gauges.

2.2.3. Distribution Characteristics of Foam Systems in Fractures of Different Sizes. In this study, the stone core holder was used as the main body of the experimental instrument, capable of withstanding temperatures up to 150 °C and pressures up to 25 MPa. It was used to fill the stone core as a medium to simulate the reservoir environment. Additionally, instruments such as steel intermediate containers, gas flow meters, drying pipes, check valves, and ISCO plunger pumps were utilized. The specific working parameters and specifications of these instruments were consistent with those used in previous studies.

2.3. Experimental Methods and Procedures. *2.3.1. Formation Characteristics of Foam Systems in Fractures with Different Roughness.* Before the formal experiment, an experimental system was established, as shown in Figure 5. The 80 and 120 mesh glass microspheres were filled into the model fracture mesh to create different simulated reservoir fracture environments. The fracture edge near the inlet and outlet of the model fluid was designed as a semicircle to reduce

Figure 4. Diagram of the ultradepth field 3D microscope.

https://doi.org/10.1021/acsomega.3c10510
ACS Omega 2024, 9, 24362−24371

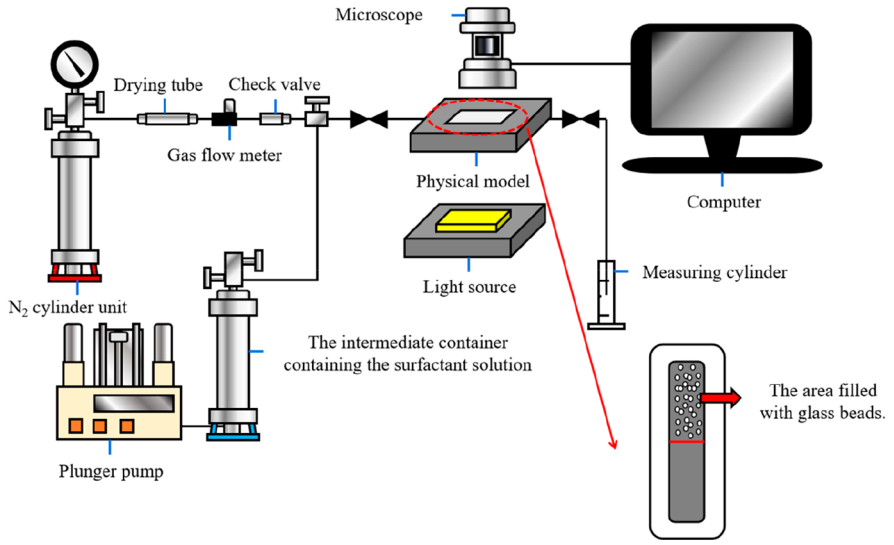

Figure 5. Schematic diagram of the experimental system for foam formation characteristics.

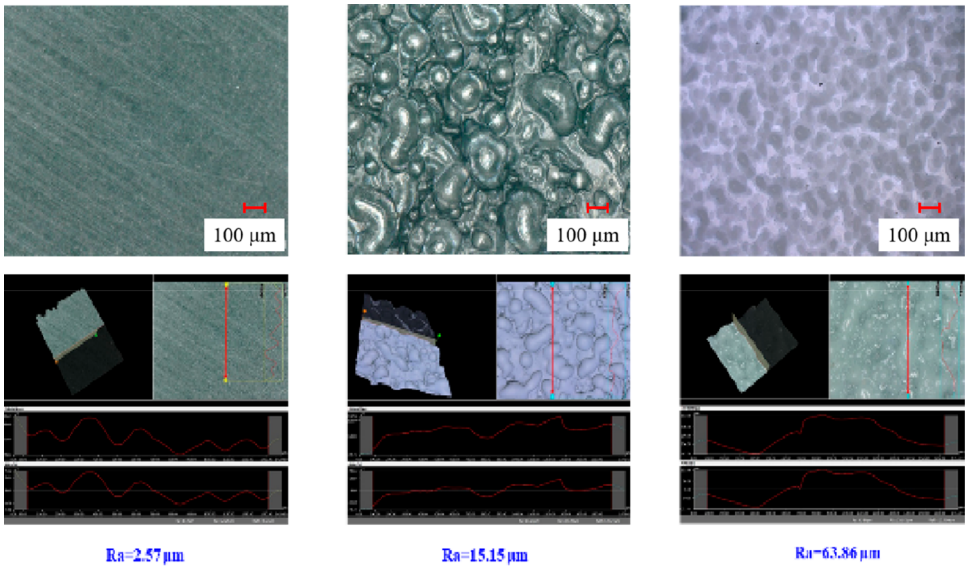

Figure 6. Roughness of the simulated crack measured by the instrument.

flow loss.[27−31] The fluid injection end of the model bottom plate was filled with glass microbeads. The filling range was bounded by the central axis of the long side of the fluid flow space in the model. The changes in the roughness of the real fracture wall were simulated by changing the diameter of the filled glass microbeads. Subsequently, the reservoir physical model was placed in an environment with a constant temperature of 25 °C. During the formal experiment, the foam flooding process was carried out, and the pressure-reducing valve, drying pipe, gas flow meter, and check valve were connected at the outlet of the nitrogen gas source in turn. Nitrogen and surfactant solutions were injected into the model at different gas−liquid ratios. The total injection rate of the mixture fluid of nitrogen and surfactant was 1 mL·min^{-1}. In addition, the concentration of the surfactant solution was set to 0.2 wt %. The flow of fluid in the model was observed during oil displacement.

2.3.2. Migration Characteristics of Foam Systems in Fractures with Different Roughness. In this study, surface roughness refers to the unevenness between the small peaks and valleys on the fracture wall, which belongs to the category of surface morphological changes at the microscopic level. Therefore, the surface roughness is usually measured by optical methods such as optical cutting microscope and interference microscope.[32−35] To evaluate the surface roughness of the model cavity wall in this study, the contour arithmetic mean deviation R_a was introduced, which refers to the arithmetic average of the distance between each point deviating from the center in a certain length range. In practical measurements, it was common to conduct more measurements at certain points and obtain a relatively accurate R_a by calculating the average value, to measure the roughness of the wall surface.[36] Figure 6 shows the surface roughness of three different materials measured by an optical microscope after deep scanning. Their deviation heights from smooth to rough were 2.57, 15.15, and 63.86 μm successively.

In the formal experimental stage, the experimental system was established according to the process shown in Figure 7.

https://doi.org/10.1021/acsomega.3c10510
ACS Omega 2024, 9, 24362−24371

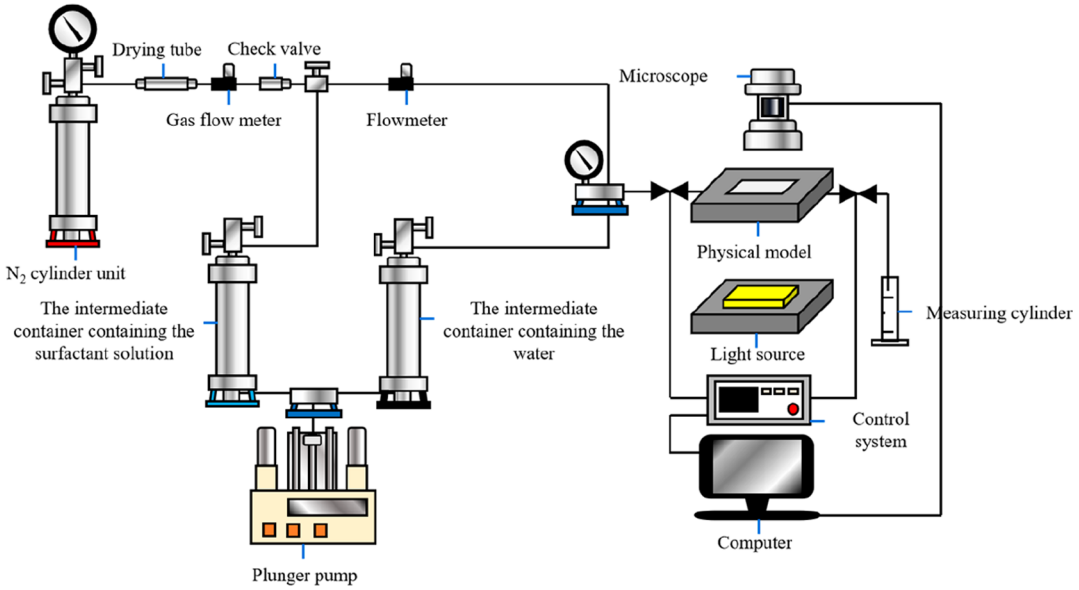

Figure 7. Schematic diagram of the experimental system for foam migration characteristics.

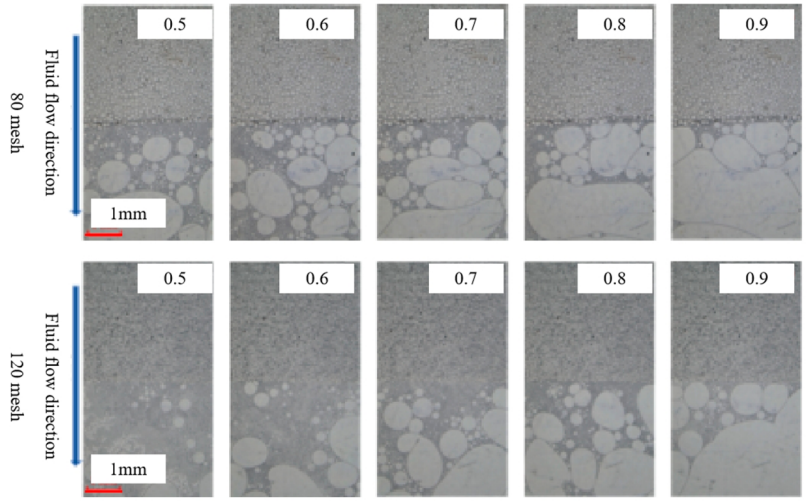

Figure 8. Formation of foam with different qualities in fractures.

First, a sufficient amount of surfactant solution with a mass concentration of 0.2 wt % was prepared, and the air tightness of the device was checked.[37−39] During the experiment, the gas−liquid ratio of the fluid injected into the model was controlled to change the foam quality. The total flow rate of gas and liquid was set as 1 mL·min^{-1}, and the flow law of the foam in the fracture was observed. When the pressure stabilized, the pressure representation number was recorded, that is, the foam flooding pressure difference at this time, and the resistance effect caused by the simulated fracture in the reservoir model was evaluated with this parameter.[38] After the flow resistance test in the smooth fracture was completed, the inner cavity of the model was opened, and cellophane with the R_a of 2.57 μm, R_a of 15.15 μm, and R_a of 63.86 μm were placed inside the model, respectively, and foam flooding with different foam qualities was performed again at the same total fluid injection rate as in the previous part of the foam flooding stage.[40,41] The flow resistance of foam under different fracture roughness conditions was measured. After the completion of the above experimental steps, the cellophane with R_a = 63.86 μm was placed at half the length of the fracture of the cavity of the physical model, and the other fracture locations were reserved as smooth walls. Then, foam flooding was carried out, the gas/liquid ratio was 2:1, and the total fluid injection rate was 0.05 mL·min^{-1}. The influence of roughness changes on foam flow in the fracture was studied, and the pictures were recorded by the microscope. In addition, after the end of each group of experiments, the fracture model was washed with ultrapure water to remove the residue inside the model for the next group of experiments.

2.3.3. Distribution Characteristics of Foam Systems in Fractures with Different Sizes. The purpose of studying the formation and migration mechanism of foam injected into the reservoir was to effectively seal the high permeability fractures, adjust the injection profile, and create conditions for improving the sweep efficiency of subsequent injection fluids and optimizing final oil recovery.[42−44] Therefore, to verify the effectiveness of the foam plugging mechanism in the fracture environment, stone core flooding experiments were designed. During the experiment, gas flooding and foam flooding were

https://doi.org/10.1021/acsomega.3c10510
ACS Omega 2024, 9, 24362−24371

conducted on each stone core model, with the small fracture with an opening of 0.09 mm serving as the foundation. The flow rate changes of foam in combinations of this small fracture with fractures with openings of 0.4 0.8, and 1.2 mm were compared. The experimental implementation process was similar to the system and scheme used in the previous part of the work, divided into pregas flooding and foam flooding in the second stage. The difference was that the physical model was replaced by two groups of stone core grippers equipped with two kinds of stone core fractures with different opening degrees.[45−47] The stone core grippers were arranged in parallel in the experimental system. The flow rate of the fluid passing through the two types of stone cores in the displacement process was measured separately, and the flow separation rate of the microfracture with a small opening was calculated.

3. RESULTS AND DISCUSSION

3.1. Formation Characteristics of Foam Systems in Fractures with Different Roughness. In this experiment, a visual fracture model with an opening of 200 μm was utilized to observe the flow characteristics and regeneration of the foam under various conditions. The gas volume ratio range of the injected gas−liquid mixed fluid was set between 0.5 and 0.9. Figure 8 displayed the formation of foam as the fluid passed through the visual microscopic fracture model, with the gas volume ratio of the injected mixed fluid indicated in the image. Figure 9 depicts the changes in the microstructure of

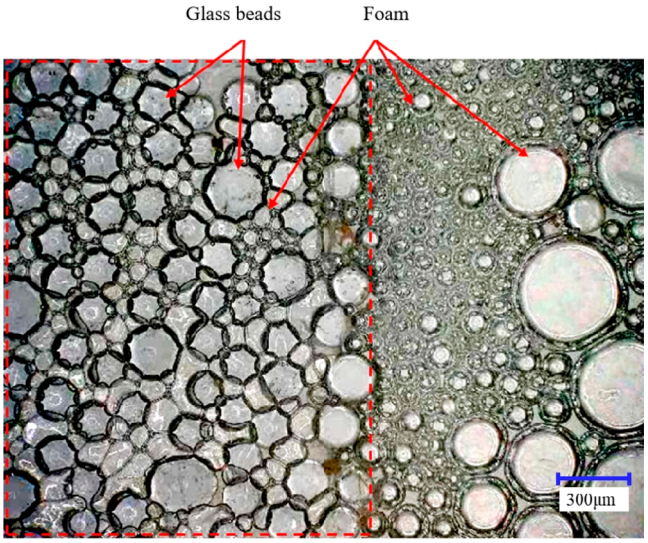

Figure 9. Cutting effect of the rough parts of fracture on bubbles promotes the differentiation and regeneration of foam.

the liquid film as the fluid flowed through the filling site of glass microspheres in the model, as captured by an optical super depth-of-field microscope.

According to the comprehensive analyses of Figure 8 and Figure 9, it was observed that bubbles of various sizes and shapes were generated after the injected gas−liquid mixed fluid passed through the high-roughness region filled with glass microspheres. When there was a flowing foam liquid film at a certain flow rate, the film broke at any surface protrusion in the flow space, forming multiple bubbles. As a large bubble passed through two larger protrusions of the fracture, it was squeezed and deformed, leading to changes in capillary pressure. When the capillary pressure was lower than the critical value, the elongated and deformed bubbles underwent necking separation in the narrow part of the flow space, resulting in the differentiation of large bubbles into small bubbles. Under the condition of the same roughness of the fracture wall, the average diameter of the bubbles gradually increased with the increase of the gas phase content of the injected fluid, and the irregular shape of the bubbles also increased. Due to the gas−liquid slippage effect, a large number of gases could not effectively participate in the bubble formation process but quickly broke through to the edge of roughness change and combined with the liquid film to form large bubbles. The foam produced in the model filled with 120 mesh glass microspheres was denser, and the number of small bubbles was higher when the gas phase content of the mixed fluid was the same. Glass microspheres with a higher mesh number had smaller sizes, and the protrusions formed on the fracture wall were relatively small and uniform. When the foaming agent liquid film and gas flowed simultaneously, the cutting effect of the rough part on the fracture surface was more frequent, resulting in relatively smaller diameters of the bubbles generated by differentiation and regeneration, making the resulting foam denser. The densification of the foam structure was conducive to the stable flow of the system in the fractured environment of the reservoir and strengthened the implementation of a series of fracture plugging effects and fluid flow control effects, which had a positive effect on the optimization of reservoir development benefits. Thus, foam improved the development process for reservoirs with complex fracture structures as well as small fracture structures.

3.2. Migration Characteristics of Foam Systems in Fractures with Different Roughness. The effects of foam quality and foam flow resistance were investigated by injecting the foam into the fracture model at a constant total volume flow rate of 1.0 mL·min^{-1}. Figure 10 illustrates the variation of the pressure drop during foam injection in the model with different fracture wall roughness. The results show that the differential pressure of the system decreases with the increase in the liquid retention rate of the foam. It can be seen that the increase in the amount of liquid in the system will reduce the

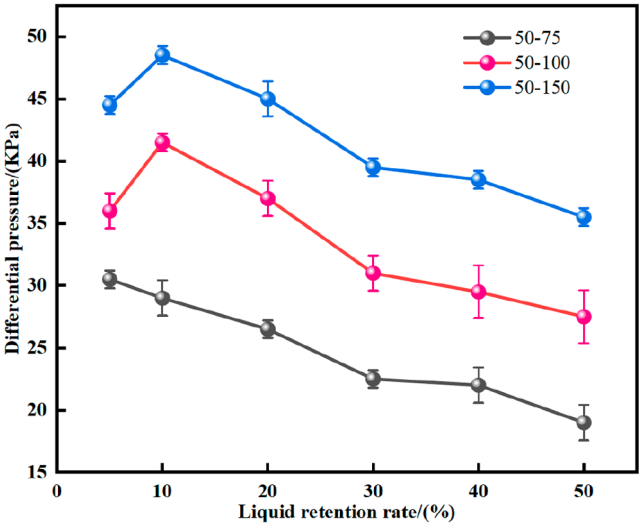

Figure 10. Flow pressure difference produced by the foams with different liquid retention rates in fractures with different opening degrees.

https://doi.org/10.1021/acsomega.3c10510
ACS Omega 2024, 9, 24362−24371

mechanical strength of the system, resulting in a weakening of its fracture-sealing effect.

Figure 11 shows the flow resistance of foam with different qualities in models with different fracture roughness. Under the

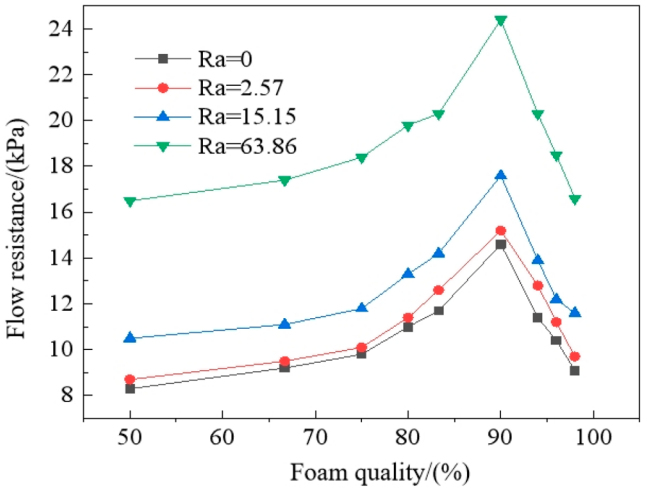

Figure 11. Flow resistance produced by the foams with different qualities in fractures with different roughness.

condition that the foam quality increased from 50% to 98% and the roughness of the roughest wall surface was 63.86 μm, it could be observed from Figure 11 that the flow resistance of the foam increased with the increase of the foam quality within the range of 50%−90%. However, when the foam quality was in the range of 90%−98%, the flow resistance decreased rapidly with further increases in foam quality. Additionally, under the same flow velocity and foam quality, the flow resistance of the foam also increased with fracture roughness. For example, when the foam quality was 90%, the seepage resistance of the foam in the smooth flat fracture was 14.6 kPa. When the surface of the fracture was coated with cellophane (R_a = 63.86 μm), the flow resistance of the foam rose to 24.4 kPa, which was almost twice the resistance of the foam in the smooth flat fracture. Therefore, the results indicated that there existed an optimal foam quality level in foam injection operations to maximize the plugging effect of the foam. Below this optimal foam quality, the space for the system to exert the plugging effect was limited due to the small number of bubble structures in the foam. Conversely, above this optimal foam quality, the bubble liquid film was thin, leading to a fragile system structure that was not conducive to its plugging effect improvement. Therefore, in actual injection processes, it was necessary to consider field conditions to determine the appropriate injected foam quality, thereby optimizing the oil displacement of the foam and the fluid sweep efficiency.

Subsequently, the average diameter of the foam in fractures with varying roughness was recorded using a microscope, and the results are shown in Figure 12. The data show that the average diameter of bubbles in the foam decreases with the increase of the liquid retention rate of the system. The liquid retention rate represents the amount of liquid in the system, and an increase in the amount of liquid provides conditions for the formation of more foam liquid films in the system, resulting in a stronger division of the gas phase, resulting in the formation of smaller bubbles. Figure 13 illustrates the flow process of foam from rough fractures to smooth fractures,

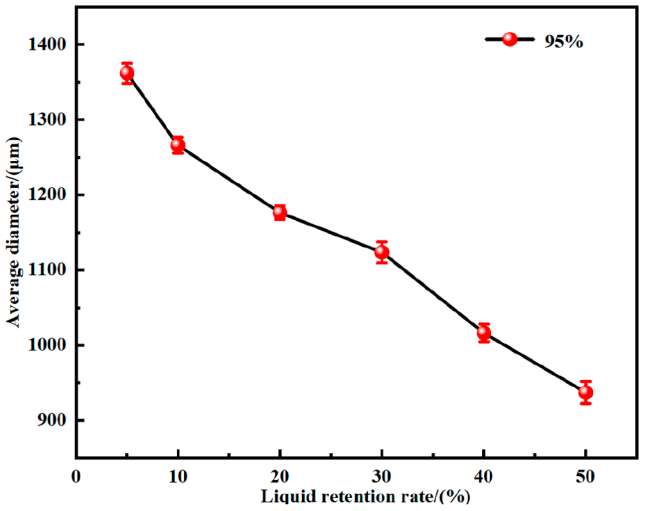

Figure 12. Equivalent diameters of bubbles in the foams with different liquid retention rates.

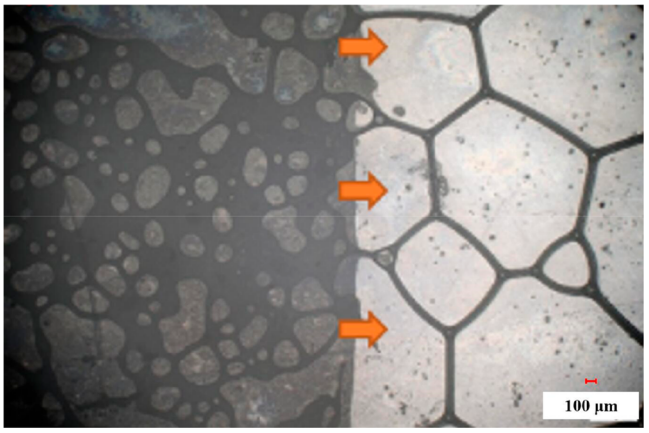

Figure 13. Microstructure of foam in fractures with different roughness.

moving from regions of high flow resistance to low flow resistance. The arrows in the figure describe the flow direction of the fluid. In the first half of the model, in the rough wall fracture area, the roughness of the fracture wall caused the distance between the wave peaks on the surface to be smaller than the size of the foam generated. As a result, the foam needed to constantly deform to pass through the rough wall. This deformation, combined with the Jamin effect, significantly increased the flow resistance of the foam. Additionally, particles in the convex part of the rough wall could effectively shear the foam, causing large bubbles to differentiate into several small bubbles, which further required a portion of the pressure energy during the fluid migration process to push these bubbles. Under this condition, the system generated greater fluid flow resistance, and the plugging effect of the foam was better.

When the foam flowed from a zone with high flow resistance to a zone with low flow resistance, the impact of changes in the foam structure was depicted in Figure 14. During the migration of the foam fluid from a fracture surface with a roughness (R_a) of 63.86 μm to a smoother fracture surface, a noticeable change in the foam property occurred at the junction where the fracture roughness shifts. As the foam moved along the smoother surface, the frequency of the shearing effect of the

https://doi.org/10.1021/acsomega.3c10510
ACS Omega 2024, 9, 24362−24371

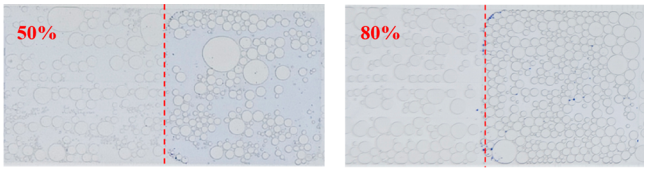

Figure 14. Flow of foams with different qualities. (The foam flows from the high permeability zone to the low permeability zone.)

fracture wall on the foam surface decreased due to the decrease in surface inhomogeneity, resulting in a significant increase in the size of the foam bubbles and enhanced stability of the foam structure.

Figure 15 illustrates the migration process of the foam from a zone with high seepage resistance to a zone with low seepage

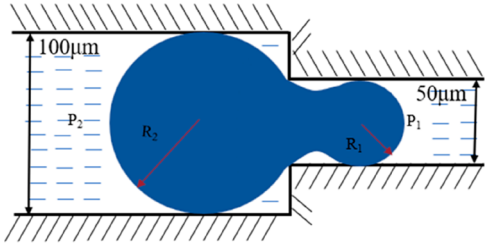

Figure 15. Change of force caused by the change of foam at the change of fracture opening.

resistance. In smooth fractures, the average particle size of the foam was relatively large. When the foam migrated from low-roughness fractures to high-roughness fractures, bubbles continuously accumulated at the interface where the fracture roughness changed due to the interference of the increased protrusions on the fracture surface, leading to significant liquid film deformation and bubble shearing phenomena. Eventually, the foam flowed into the rough wall, where foam differentiation is more pronounced. As shown in Figure 15, regardless of whether the foam flowed from a low-permeability fracture to a high-permeability fracture or vice versa, the variation in roughness enhanced the regeneration and differentiation of the foam system, maintaining the foam stability. The foam in complex fracture environments underwent more active splitting and regeneration due to increased shear disturbances from external forces, ensuring that the strength and stability of the foam structure maintain dynamic equilibrium over time. This was beneficial for the development of foam profile control mechanisms and plugging effects, ultimately improving the efficiency of the injected fluid sweep and optimizing the oil recovery.

3.3. Distribution Characteristics of Foam Systems in Fractures with Different Sizes. The displacement pressure difference generated by each foam flow in fractures with different sizes is shown in Figure 16. The flow resistance of fluids in fractures with large openings was smaller, and the corresponding displacement pressure difference was lower. The pressure difference of foam flooding was greater than that of gas flooding in the fractures with different opening environments. It could be seen that the superimposed Jamin effect of the foam based on the bubble liquid film structure in the reservoir fracture environment increases the flow resistance of the gas and effectively inhibits its channeling out of the reservoir through high-permeability channels, which played a positive role in improving the sweep efficiency of the injected

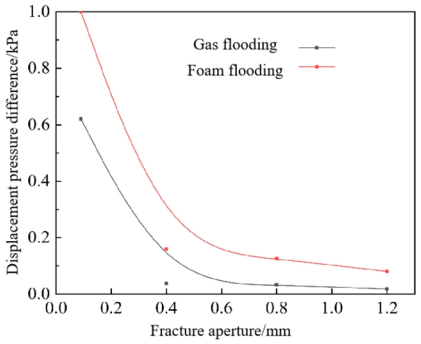

Figure 16. Displacement pressure difference of various fluids in fractures with different opening degrees.

gas and the process of oil displacement. In addition, the lower the fracture opening, the larger the gap between the displacement pressure difference between foam flooding and water flooding. It could be seen that in the low permeability reservoir which had a small fracture with a low fracture opening, the intensity of a series of injection or production profile adjustment effects brought by foam based on the plugging effect was more obvious, reflecting the superiority of the foam flooding technology system in the development of reservoirs with a variety of complex fracture structures and low permeability fracture areas.

Subsequently, the flow conditions of fluids in fractures with different opening degrees were compared, and the experimental results are shown in Figure 17. It could be seen that

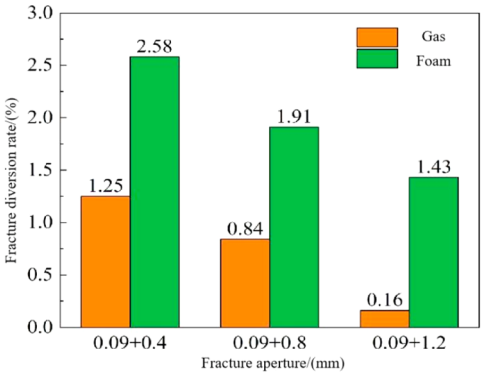

Figure 17. Fluid diversion rate under different fracture opening combinations.

the presence of the fractures with the large opening had a strong shielding effect on the flow of fluid to the fractures with the small opening and the larger the gap between the openings of the two kinds of fractures, The more obvious was the difference in the flow diversion between them, that is, the smaller the opening of the fracture, the smaller the diversion rate of the fluid in the fracture. This showed that the greater the difference in reservoir permeability, the more likely it was that injected fluid would flow to high-permeability and large-size fractures during the injection process of reservoir development, which would accelerate the generation of channeling and the phenomenon of fluid channeling. The more heterogeneous reservoir environment was more likely to provide conditions for the formation of the fluid channeling phenomenon. However, the experimental data also showed that the flow diversion rate of low-opening fractures in the

https://doi.org/10.1021/acsomega.3c10510
ACS Omega 2024, 9, 24362−24371

foam flooding stage is significantly higher than that in the gas flooding stage. This law showed that the liquid film structure of the foam effectively wrapped the nitrogen gas and sealed the hyperpermeability in the stone core simulated reservoir based on the resistance brought by the superimposed Jamin effect, thereby squeezing the subsequently injected fluid into the small-opening fractures of the reservoir, which were difficult for the conventional fluids to enter. This process gradually eliminated the shielding behavior of the fluid flow in the high permeability fracture, optimized the sweep efficiency of the injected fluid, improved the sweep efficiency of the fluid, and created a foundation for the improvement of oil recovery and the improvement of reservoir development benefits.

4. CONCLUSION

(1) Compared with the high permeability reservoir, the low permeability reservoir can exert a stronger shear effect on the injected foam due to its fractures with the more complex structure and the smaller volume, thus producing dense foam with smaller bubbles that have a smaller size. The low permeability reservoir is conducive to the formation of high-strength foam and its implementation of a series of effects to improve fluid sweep efficiency and optimize oil recovery.

(2) The foam encloses the gas phase through its liquid film; thus, the preferential migration passage is plugged by the superposition of the Jamin effect caused by this film. The resulting resistance effect forces the subsequently injected fluid into the low permeability fractures that were previously difficult to sweep, to break through the shielding effect of high permeability fracture on low permeability fracture, and the fluid diversion rate of the latter is increased. Under this condition, fluid channeling is inhibited, and foam sweep efficiency is improved effectively, which creates conditions for the improvement of oil recovery.

(3) The higher the roughness of the reservoir fracture, the stronger the shear disturbance effect caused by the reservoir on the injected fluid, which contributes to the regeneration of the foam and the increase in the flow resistance of the foam. These conditions help foam to plug the high permeability preferential migration passage and optimize the fluid sweep efficiency, which reflects the superiority of foam flooding in the development of reservoirs with complex fracture structures and low permeability.

(4) The foam in the best quality state can maximize its blocking effect on the high permeability fractures of the reservoir. When the foam quality is lower than the optimal quality, the space for the system to plug the fracture is limited due to the less bubble liquid film structure in the foam. When the foam quality is higher than the optimal quality, the bubble liquid film becomes thin and the system structure is weak, which is not conducive to its fracture plugging sealing effect.

AUTHOR INFORMATION

Corresponding Authors

Zhengxiao Xu − *School of Petroleum and Natural Gas Engineering, Changzhou University, Changzhou 213164, PR China;* orcid.org/0000-0002-8849-3406; Email: xzx@cczu.edu.cn

Chao Zhang − *Key Laboratory of Unconventional Oil & Gas Development (China University of Petroleum (East China)), Ministry of Education, Qingdao 266580, PR China; School of Petroleum Engineering, China University of Petroleum (East China), Qingdao 266580, PR China;* orcid.org/0000-0001-7914-0716; Email: zhangc@upc.edu.cn

Authors

Jinghui Li − *Sinopec Northwest Company of China Petroleum and Chemical Corporation, Xinjiang 830011, PR China; Sinopec Key Laboratory of Enhanced Oil Recovery for Fractured Vuggy Reservoirs, Xinjiang 830011, PR China*

Yibo Feng − *Sinopec Northwest Company of China Petroleum and Chemical Corporation, Xinjiang 830011, PR China; Sinopec Key Laboratory of Enhanced Oil Recovery for Fractured Vuggy Reservoirs, Xinjiang 830011, PR China*

Jianhai Wang − *Sinopec Northwest Company of China Petroleum and Chemical Corporation, Xinjiang 830011, PR China; Sinopec Key Laboratory of Enhanced Oil Recovery for Fractured Vuggy Reservoirs, Xinjiang 830011, PR China*

Binfei Li − *Key Laboratory of Unconventional Oil & Gas Development (China University of Petroleum (East China)), Ministry of Education, Qingdao 266580, PR China; School of Petroleum Engineering, China University of Petroleum (East China), Qingdao 266580, PR China*

Complete contact information is available at: https://pubs.acs.org/10.1021/acsomega.3c10510

Notes

The authors declare no competing financial interest.

ACKNOWLEDGMENTS

This research was funded by the National Natural Science Foundation of China (52204068 and U20B6003). We are grateful to the Shandong Engineering Research Center for CO_2 Utilization and Storage for their kind help in this study. The valuable comments made by the anonymous reviewers are also sincerely appreciated.

REFERENCES

(1) Li, H.; Gao, Y.; Chen, A. Application and development trend of foam system in oilfield. *Progress in fine petrochemicals* **2010**, *11* (2), 22−26.

(2) Friedmann, F.; Chen, W. H.; Gauglitz, P. A. Experimental and simulation study of high-temperature foam displacement in porous media. *SPE Reservoir Engineering* **1991**, *6* (1), 37−45.

(3) Zhang, C.; Gu, Z.; Cao, L.; Wu, H.; Liu, J.; Li, P.; Zhang, D.; Li, Z. Effect of Pressure and Temperature Variation on Wax Precipitation in the Wellbore of Ultradeep Gas Condensate Reservoirs. *SPE Journal* **2024**, *29*, 1589−1604.

(4) Pang, Z.; Cheng, L.; Chen, Y. Study on nitrogen foam control technology of water cone in conventional heavy oil bottom water reservoir. *Acta Petrolei Sinica* **2007**, *28* (5), 99−103.

(5) Guo, P.; Li, S.; Du, Z. Evaluation of enhanced oil recovery by gas injection in low permeability reservoirs. *Journal of Southwest Petroleum University, Natural Science Edition* **2002**, *24* (5), 46−50.

(6) Fu, J.; Zhang, L.; Yin, D. Plugging and profile control performance of reinforced foam and field test. *Oil and gas geology and recovery* **2005**, *12* (5), 47−49.

(7) Liu, Y.; Rui, Z.; Yang, T.; Dindoruk, B. Using Propanol as an Additive to CO_2 for Improving CO_2 Utilization and Storage in Oil Reservoirs. *Applied Energy* **2022**, *311*, 118640.

(8) Wang, M.; Guo, D. Foaming properties of foams and its influencing factors. *Progress in fine petrochemicals* **2007**, *12*, 40.

https://doi.org/10.1021/acsomega.3c10510
ACS Omega 2024, 9, 24362−24371

(9) Cheng, H.; Yuan, F.; Zhang, S.; Li, L.; Luo, X.; Chen, B. Investigation on Water Invasion Mode and Remaining Oil Utilization Rules of Fractured-Vuggy Reservoirs: A Case Study of the Intersection Region of S99 Unit in Tahe Oilfield. *Processes* **2023**, *11* (6), 1833.
(10) Li, G.; Mou, J.; Sui, H. Study on dynamic surface tension and adsorption kinetics of surfactant solution (continued). *Household chemical industry* **2006**, *1999* (05), 3−5.
(11) Li, Y.; Peng, G.; Tang, J.; Zhang, J.; Zhao, W.; Liu, B.; Pan, Y. Thermo-hydro-mechanical coupling simulation for fracture propagation in CO_2 fracturing based on phase-field model. *Energy* **2023**, *284*, 128629.
(12) Zhang, C.; Liu, Y.; Gu, Z.; Li, P.; Li, Z.; Zhang, K. Chemicals-CO_2 mechanisms of inhibiting steam heat transfer and enhancing oil film strip: Steam flow through the wall-adhering oil film surface in porous medium. *Fuel* **2024**, *356*, 129572.
(13) Ju, Y.; Tang, S.; Zhou, Y. Effect of cation on adsorption of sodium dodecyl benzene sulfonate on Illite. *Oilfield chemistry* **1992**, *1*, 62.
(14) Xiao, J.; Cui, Y.; Fan, H. Preparation and principle of Ph-sensitive hydrogels. *Henan Chemical Industry* **2003**, *8*, 5−7.
(15) Liu, Y.; Ma, X.; Li, H. A.; Hou, J. Competitive adsorption behavior of hydrocarbon(s)/CO_2 mixtures in a double-nanopore system using molecular simulations. *Fuel* **2019**, *252*, 612−621.
(16) Wan, L.; Meng, Y.; Zhao, X. Study on the stability mechanism of foam fluid. *Journal of Xinjiang Petroleum Institute* **2003**, *1*, 70−73.
(17) Gu, Z.; Zhang, C.; Lu, T.; Wang, H.; Li, Z.; Wang, H. Experimental analysis of the stimulation mechanism of CO_2-assisted steam flooding in ultra-heavy oil reservoirs and its significance in carbon sequestration. *Fuel* **2023**, *345*, 128188.
(18) Wang, B.; Zhou, M.; Tang, X. Screening and stability study of temperature - and salt-resistant foaming agent system for pressure cone. *Inner Mongolia petrochemical industry* **2015**, *2*, 5−7.
(19) Zhang, C.; Xi, L.; Wu, P.; Li, Z. A novel system for reducing CO_2-crude oil minimum miscibility pressure with CO_2-soluble surfactants. *Fuel* **2020**, *281*, 118690.
(20) Kang, W.; Wang, J.; Wu, X. Study on the stability and influencing factors of amphiphilic polymer foam. *Oilfield chemistry* **2012**, *29* (1), 48−51.
(21) Li, Y.; Hubuqin; Wu, J.; Zhang, J.; Yang, H.; Zeng, B.; Xiao, Y.; Liu, J. Optimization method of oriented perforation parameters improving uneven fractures initiation for horizontal well fracturing. *Fuel* **2023**, *349*, 128754.
(22) Jiang, J.; Yue, X.; Gao, Z. The role of polymer in the modulation and flooding of foam composite. *Oil drilling and production technology* **2011**, *33* (1), 61−64.
(23) Rao, P.; Yang, H.; Pu, C. Simulation application research of air foam/gel composite flooding technology in shallow ultra-low permeability and low temperature reservoirs. *Applied chemical industry* **2012**, *41* (11), 1868−1871.
(24) Cheng, H.; Jiang, L.; Li, C. Experimental Study on Production Characteristics of Bottom Water Fractured-Vuggy Reservoir. *Geofluids* **2022**, *2022*, 2022.
(25) Liu, Y.; Li, H. A.; Okuno, R. Measurements and Modeling of Interfacial Tension of CO_2-CH_4-brine System at Reservoir Conditions. *Ind. Eng. Chem. Res.* **2016**, *55* (48), 12358−12375.
(26) Li, D.; Ren, B.; Zhang, L.; Ezekiel, J.; Ren, S.; Feng, Y. CO_2-sensitive foams for mobility control and channeling blocking in enhanced WAG process. *Chem. Eng. Res. Des.* **2015**, *102*, 234−243.
(27) Zhang, C.; Wu, P.; Li, Z.; Liu, T.; Zhao, L.; Hu, D. Ethanol enhanced anionic surfactant solubility in CO_2 and CO_2 foam stability: MD simulation and experimental investigations. *Fuel* **2020**, *267*, 117162.
(28) Binks, B.P.; Fletcher, P.D.I.; Tian, L. Influence of nanoparticle addition to winsor surfactant microemulsion systems. *Colloids and Surface A: Physicochemical and Engineering Aspects* **2010**, *363* (6), 8−15.
(29) Tang, B.; Geng, C.; Huang, M.; Lu, H.; Ren, K. Research on the Depletion and Recovery Characteristics of Fault-Karst Reservoirs. *Geofluids* **2022**, *2022*, 2022.
(30) Liu, F. Research and application of high temperature three phase foam system. *Laboratory science* **2006**, *11* (6), 49−51.
(31) Liu, Y.; Hou, J. Selective Adsorption of CO_2/CH_4 Mixture on Clay-rich Shale using Molecular Simulations. *Journal of CO_2 Utilization* **2020**, *39*, 101143.
(32) Li, Y.; Li, M.; Tang, J. A hydraulic fracture height mathematical model considering the influence of plastic region at fracture tip. *Petroleum Exploration and Development* **2020**, *47* (1), 184−195.
(33) Wang, H.; Lun, Z.; Lv, C.; Lang, D.; Luo, M.; Zhao, Q.; Zhao, C. Nuclear-magnetic-resonance study on oil mobilization in shale exposed to CO_2. *SPE Journal* **2020**, *25* (01), 432−439.
(34) Zhang, C.; Li, Z.; Sun, Q.; Wang, P.; Wang, S.; Liu, W. CO_2 foam properties and the stabilizing mechanism of sodium bis (2-ethylhexyl) sulfosuccinate and hydrophobic nanoparticle mixtures. *Soft Matter* **2016**, *12* (3), 946−956.
(35) Cheng, H. The Enhanced Oil Recovery Effect of Nitrogen-Assisted Gravity Drainage in Karst Reservoirs with Different Genesis: A Case Study of the Tahe Oilfield. *Processes* **2023**, *11* (8), 2316.
(36) Liu, X.; Du, R.; Yang, T. Low temperature synthesis and properties of salt-resistant polymer gels. *Journal of Materials Science and Engineering* **2016**, *34* (04).
(37) Tang, B.; Ren, K.; Lu, H.; Li, C.; Geng, C.; Wei, L.; Chai, Z.; Wu, S. Study on residual oil distribution law during the depletion production and water flooding stages in the fault-karst carbonate reservoirs. *Processes* **2023**, *11* (7), 2147.
(38) Dai, C.; Zhao, G.; Zhao, M.; You, Q. Preparation of dispersed particle gel (DPG) through a simple high speed shearing method. *Molecules* **2012**, *17* (12), 14484−14489.
(39) Liu, P.; Jiang, L.; Tang, B.; Ren, K.; Huang, M.; Geng, C. Residual oil distribution pattern in a fault-solution carbonate reservoir and countermeasures to improve oil development effectiveness. *Geofluids* **2022**, *2022*, 1.
(40) Wang, H.; Lun, Z.; Lv, C.; Lang, D.; Pan, W.; Luo, M.; Wang, R.; Chen, S. Nuclear-magnetic-resonance study on mechanisms of oil mobilization in tight sandstone reservoir exposed to carbon dioxide. *SPE Journal* **2018**, *23* (03), 750−761.
(41) Wang, S.; Feng, Q.; Javadpour, F.; Hu, Q.; Wu, K. Competitive adsorption of methane and ethane in montmorillonite nanopores of shale at supercritical conditions: A grand canonical Monte Carlo simulation study. *Chemical Engineering Journal* **2019**, *355*, 76−90.
(42) Dai, C.; Zhao, G.; Zhao, M.; You, Q. Preparation of dispersed particle gel (DPG) through a simple high speed shearing method. *Molecules* **2012**, *17* (12), 14484−14489.
(43) Cong, Z.; Li, Y.; Pan, Y.; Liu, B.; Shi, Y.; Wei, J.; Li, W. Study on CO_2 foam fracturing model and fracture propagation simulation. *Energy* **2022**, *238*, 121778.
(44) Liu, Y.; Rui, Z. A Storage-Driven CO_2 EOR for Net-zero Emission Target. *Engineering* **2022**, *18*, 79−87.
(45) Zhang, C.; Gu, Z.; Li, P.; et al. Investigation on the condensate gas composition variation and wax deposition mechanism during temperature-induced phase transition process. *Journal of Cleaner Production* **2024**, *442*, 141109.
(46) Yuqiang, X.; Yucong, W.; Yang, T.; Pinyaeva, T.; Zhichuan, G. Experimental study on ultrasonic wave propagation characteristics of gas-liquid two-phase flow in riser annulus. *Applied Ocean Research* **2023**, *141*, 103771.
(47) Xu, Y.; Li, F.; Li, Q.; Wang, Y.; Nie, J.; Yang, L. Numerical simulation method and structural optimization for shearing capacity of ram blowout preventers. *Geoenergy Science and Engineering* **2024**, *233*, 212559.

https://doi.org/10.1021/acsomega.3c10510
ACS Omega 2024, 9, 24362−24371